



CrossMark  
click for updates

Cite this: *RSC Adv.*, 2016, 6, 103137

# Cationic porphyrin@SPION nanospheres as multifunctional anticancer therapeutics: magnetic targeting, photodynamic potential and bio-safety research†

Ping Zhao,<sup>\*ab</sup> Min-Chao Liu,<sup>a</sup> Thushara W. Madanayake,<sup>b</sup> Chawla Reena,<sup>b</sup> Min Zheng,<sup>c</sup> Zhen-Feng Cheng,<sup>a</sup> Yu-Min Huang<sup>a</sup> and Xia-Hong Wang<sup>a</sup>

The synthesis and characterization of carboxyl-functionalized superparamagnetic iron oxide nanoparticles (SPION)-attached cationic porphyrins with different positive charges (porphyrin@SPION) are described as pH-sensitive, multifunctional photosensitization. These nanospheres exhibit excellent targeted cell accumulation under external magnetic field and outstanding cell photocytotoxicity in weak acidic solution, which is the pH for most tumors. The dicationic porphyrin@SPION has the smartest pH-responding release and lowest half-maximal inhibitory concentration (IC<sub>50</sub>) values after visible light irradiation against HeLa cells. Moreover, the delivery safety of these porphyrin@SPION nanospheres was considered by investigating their behaviors in human plasma during the delivery process. The results elucidate that these nanospheres have no significant deleterious influence on the frame conformation of protein in their delivery process and thus are relatively safe in the drug delivery process. Our study demonstrates that the combination of targeted magnetic-loading drug design methodology with the PDT potential of cationic porphyrins may be a very useful strategy to develop novel tumor-oriented multifunctional anticancer therapeutics.

Received 4th August 2016  
Accepted 9th October 2016

DOI: 10.1039/c6ra19697g

www.rsc.org/advances

## Introduction

In recent years, the well-described photosensitizing properties of porphyrins have led to their potential use as sensitizers and adjuvants in a variety of biomedical applications, including diagnostic imaging (*e.g.* fluorescence imaging,<sup>1</sup> magnetic resonance imaging (MRI)<sup>2</sup>), therapies (*e.g.* photodynamic therapy (PDT),<sup>3</sup> sonodynamic therapy (SDT)<sup>4</sup> and boron neutron capture therapy (BNCT).<sup>5</sup> Cationic porphyrins, represented by *meso*-tetrakis(4-*N*-methylpyridiniumyl)porphyrin (TMPyP4), have attracted special attention for their additional tight interaction and efficient photocleavage with DNA. Numerous cationic porphyrins have been designed and some of them exhibit excellent anticancer abilities.<sup>6,7</sup> Our group has also devoted great efforts to this research area and successfully contributed more than 10 series of cationic porphyrins.<sup>8–10</sup> However, most porphyrins used clinically or in preclinical development are

hydrophobic and strongly aggregate in aqueous media, which significantly reduces their therapeutic efficacy because only monomeric species are appreciably active.<sup>11</sup> Moreover, it is frequently reported that this therapeutic method, PDT, is not highly selective to tumorous tissue. One of the side effects of PDT is prolonged skin photosensitivity due to sensitizer accumulation in normal cells.<sup>12</sup> These drawbacks significantly limit the biomedical applications of porphyrin and its related compounds in PDT.<sup>13</sup>

The basic design to overcome these drawbacks is to incorporate certain factors (such as drug loading, pH controlling, bioaffinity modification, *etc.*) into a conventional sensitizer to control the competition between the accumulation in normal cells and the targeted tumor tissues. Recently, researchers have been paying more attention to smart PDT treatments of cancer by integrating drug loading technology and pH-base trigger. Li *et al.* prepared a pH-activatable smart nanoparticle by adsorbing a cationic photosensitizer of *meso*-tetra(*N*-methyl-4-pyridyl) porphine (TMPyP) onto the surface of SiO<sub>2</sub> or TiO<sub>2</sub> nanoparticles.<sup>12,14</sup> Wang, Zhang and co-workers prepared a pH-responsive nanoparticle-based platform where both hydrophobic porphyrin and pH indicator bromocresol purple (BCP) were encapsulated in organically modified silica nanoparticles.<sup>15</sup> This work confirms that the use of organically modified silica nanoparticles retains both photosensitization

<sup>a</sup>School of Chemistry and Chemical Engineering, Guangdong Pharmaceutical University, No. 280, Waihuandong Road, Education Mega Centre, Guangzhou 510006, PR China. E-mail: zhaopingdpu@outlook.com

<sup>b</sup>College of Pharmacy, University of Arizona, Tucson, Arizona 85721, USA

<sup>c</sup>School of Basic, Guangdong Pharmaceutical University, No. 280, Waihuandong Road, Education Mega Centre, Guangzhou 510006, PR China

† Electronic supplementary information (ESI) available. See DOI: 10.1039/c6ra19697g

efficacy and selective accumulation in tumor cells due to the nanoporability.

However, although individuals have already shed light on incorporating nano-supporting and pH-base skills in PDT therapeutics, as far as we know, the magnetic targeting factor has not been integrated with them. Among kinds of targeted drug nano-deliverers, the superparamagnetic iron oxide nanoparticles (SPION) are particularly interesting since they are devoid of magnetic remanence due to their small size. In the last decades, SPION-based ferrofluids have been developed as contrast agents for MRI and as heating intermediates for magnetic hyperthermia. The enhanced interest of the SPION-drug associates is mostly related to the potentially combined roles of targeted therapy and diagnosis.<sup>16,17</sup>

Meanwhile, despite of the various efforts on the loading work of cationic porphyrins, currently only tetracationic TMPyP was intensively employed. The influence of positive charges on the PDT efficiency has not been considered. Herein in the present work, a series of porphyrin with different positive charges (see structures in Fig. 1) were successfully loaded on the surface of carboxyl-functionalized SPION (SPION-COOH, see schematic diagram in Fig. 2), which has deprotonated and thus negatively charged carboxylic groups at physiological pH.<sup>18</sup> The pH controlled release, cellular uptake activity, magnetic cell accumulation and photocytotoxicity of these nanospheres were comparatively studied under the pH conditions of tumor and normal cells. The number of positive charges of the porphyrin molecules were proved to have significant influence on the photocytotoxicity efficiency and dicationic porphyrin loaded on SPION-COOH exhibit even better PDT potential than TMPyP.

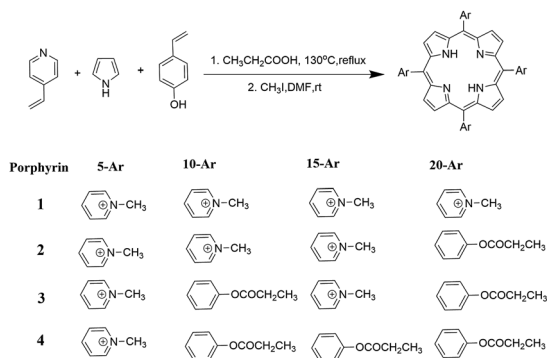


Fig. 1 The synthesis scheme of cationic porphyrins loaded on SPION.

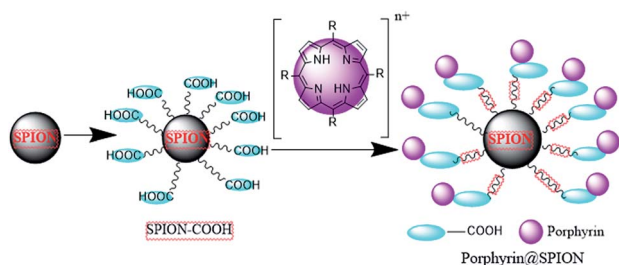


Fig. 2 The schematic diagram of porphyrin@SPION.

This contribution also concerned the bio-safety of delivery process for this system. The interactions between porphyrin@SPION and human serum albumins (HSA), which are abundantly found in blood plasma and function as carriers for numerous exogenous and endogenous compounds in the body, were investigated using the spectroscopic techniques and molecular modeling methods at the molecular level.

## Experiments

### Materials

SPION was prepared by the reported method<sup>18</sup> and porphyrins were synthesized in our lab. Succinic anhydride and triethylamine, which were used in the preparation of SPION-COOH, were obtained from J&K Chemical (China). RPMI 1640 medium, fetal bovine serum (FBS), trypsin-EDTA solution and Penicillin-streptomycin solution were purchased from Gibco Life Technologies. Water-soluble tetrazolium (WST), Hoechst 33258, and *N,N*-dimethyl-4-nitrosoaniline (RNO) were obtained from Sigma-Aldrich. Reactive Oxygen Species Assay Kit was obtained from Beyotime Biotech (China). The human blood was supplied by People's hospital of Zhongshan, Guangdong, China. All the cell lines were supplied by ATCC company of America. Human serum albumins (HSA) were obtained from Sangon Biotech (China). Measurements at fixed pH were made using 0.02 M phosphate buffer. The solutions were stored at 0–4 °C and shaken gently as needed to redissolve the contents. All the other chemicals were of analytical grade, and Millipore water (18.2 MΩ) was used throughout the experiments.

### Instrumentation

The scanning electron microscopy (SEM) analyses were performed with a JSM-6330F field emission scanning electron microscope. The transmission electron microscope (TEM) analyses were performed with a JEM-2010HR transmission electron microscope. Solid UV-Vis and FTIR spectra were recorded on a Shimadzu UV-3150 spectrophotometer and an Equinox 55 Fourier transformation infra-red spectrometer. Magnetic measurements were performed using a XL-7 magnetic property measurement system. Fluorescence microscopy of apoptosis assays was performed with an OX31 fluorescence microscope (Olympus, Japan). Electronic absorption spectroscopy was recorded on a Perkin-Elmer-Lambda-850 spectrophotometer and fluorescence spectroscopy was recorded on a Perkin-Elmer L55 spectrofluorophotometer. CD spectra were measured on a J-810 CD-Shadow spectrophotometer (Jasco, Japan). Statistical analysis was performed using origin 9.0. Comparisons between two groups were performed using unpaired *t* test. Multiple comparisons between more than two groups were performed by one-way analysis of variance. Significance was accepted at a *P* value lower than 0.05. The pH values were measured using a BeckmanpH meter (United States).

### Preparation of SPION-COOH

To a solution of 50 mg of succinic anhydride in distilled DMF, 50 mg aminated SPION nanoparticles dispersed in 10 mL DMF

were added dropwise with ultrasonication. A catalytic amount of distilled triethylamine was added to the resulting suspension and the reaction was stirred for 24 h. The particles were finally recovered by magnetic concentration, washed with distilled water and dried using acetone. SPION-COOH was thus obtained as dark brown powder.

The carboxyl groups on the surface of SPION-COOH was determined as following: to a solution of 50 mg of SPION-COOH, 20 mL 0.1 mol L<sup>-1</sup> NaHCO<sub>3</sub> solution was added. After shaking overnight, the magnetic nanospheres were removed, and 3 drops of 0.1% methyl orange solution was added to the supernatant. The supernatant was then titrated with 0.09458 mol L<sup>-1</sup> dilute hydrochloric acid solution. The carboxyl groups were thus calculated to be 18.14% according to the titration results.

### Synthesis of cationic porphyrins

Classical Adler-Longo method<sup>19</sup> was used to synthesize the porphyrins, whose synthetic pathway was given in Fig. 1.

**5,10,15,20-Tetra(*N*-methyl-4-pyridyl)porphyrin (TMPyP4, 1).** A mixture of 150 mL propionic acid, 7 mL acetic anhydride was heated at 130 °C with stirring. 2.7 mL (0.04 mol) 4-pyridinecarboxaldehyde and 3.8 mL (0.04 mol) pyrrole were then added separately from dropping funnels to the refluxing mixture. The resulting mixture was refluxed for 1.5 h. The solvent was subsequently evaporated under reduced pressure. The residue was then purified by column chromatography with CH<sub>2</sub>Cl<sub>2</sub>/EtOH = 10 : 1 as eluent. The purple powder obtained from the main band was 5,10,15,20-tetra(4-pyridyl)porphyrin, which was then methylated by an excess amount of methyl iodide afforded target compounds. Yield: 95.6%. <sup>1</sup>H NMR (500 MHz, DMSO) 9.34 (d, *J* = 6.0 Hz, 8H, 2,6-pyridinium), 9.06 (d, *J* = 7.75 Hz, 6H, 3,5-pyridinium), 8.99 (s, 8H, pyrrole), 4.72 (s, 9H, N<sup>+</sup>-Me), -3.01 (s, 2H, NH pyrrole). Anal. calcd for C<sub>44</sub>H<sub>38</sub>N<sub>8</sub>I<sub>4</sub>·4H<sub>2</sub>O: C, 41.99; H, 3.68; N, 8.90. Found: C, 42.14; H, 2.15; N, 8.99. ES-MS EtOH, *m/z*: 678 (M<sup>+</sup>), 169 (M<sup>4+</sup>). UV-Vis (10 μM in Tris buffer), λ<sub>max</sub> (nm) (log ε): 423(4.63), 517(3.39), 562(3.48), 585(3.00), 643(2.99).

**5,10,15-Tri(1-methylpyridinium-4-yl)-20-(4-methoxyphenyl)porphyrin (2).** Similar method as 1 was employed to synthesize 2, with 4-pyridinecarboxaldehyde was replaced by 2.1 mL (0.03 mol) 4-pyridinecarboxaldehyde and 1.2 g (0.01 mol) *p*-hydroxybenzaldehyde, and the eluent was replaced by CH<sub>2</sub>Cl<sub>2</sub>/EtOH = 15 : 1. The purple powder obtained from the first band was then methylated by an excess amount of methyl iodide afforded target compounds. Yield: 94.2%. <sup>1</sup>H NMR (500 MHz, DMSO): chemical shift δ: 9.34 (d, *J* = 7.75 Hz, 6H, 2,6-pyridinium), 9.06 (d, *J* = 7.75 Hz, 6H, 3,5-pyridinium), 9.01 (s, 2H, pyrrole), 8.99 (s, 6H, pyrrole), 8.27 (d, *J* = 8.41 Hz, 2H, 2,6-phenyl), 6.96 (d, *J* = 5.55 Hz, 2H, 3,5-phenyl), 4.72 (s, 9H, N<sup>+</sup>-Me), 1.27 (d, *J* = 7.71 Hz, 3H, -CH<sub>3</sub>), -2.93 (s, 2H, NH). Anal. calcd for C<sub>47</sub>H<sub>40</sub>N<sub>7</sub>I<sub>3</sub>O<sub>2</sub>·3H<sub>2</sub>O: C, 48.26; H, 3.96; N, 8.38. Found: C, 49.74; H, 4.15; N, 8.29. ES-MS EtOH, *m/z*: 734 (M<sup>+</sup>), 244 (M<sup>3+</sup>). UV-Vis (10 μM in Tris buffer), λ<sub>max</sub> (nm) (log ε): 424(5.09), 528(3.92), 559(3.70), 584(3.56), 640(3.18).

**5,15-Di(1-methylpyridinium-4-yl)-10,20-di(4-methoxyphenyl)porphyrin (3).** Similar method as 1 was employed to synthesize

3, with 4-pyridinecarboxaldehyde was replaced by 1.4 mL (0.02 mol) 4-pyridinecarboxaldehyde and 2.4 g (0.02 mol) *p*-hydroxybenzaldehyde, and the eluent was replaced by CH<sub>2</sub>Cl<sub>2</sub>/EtOH = 18 : 1. The purple powder obtained from the second band was then purified by thin layer chromatography (TCL) use CH<sub>2</sub>Cl<sub>2</sub>/EtOH = 20 : 1 as eluent to get 5,15-di(1-pyridinium-4-yl)-10,20-di(4-methoxyphenyl)porphyrin, which was then methylated by an excess amount of methyl iodide afforded target compounds. Yield: 93.7%. The spectroscopic results obtained from <sup>1</sup>H NMR (500 MHz, DMSO): chemical shift δ: 9.34 (d, *J* = 7.75 Hz, 4H, 2,6-pyridinium), 9.04 (d, *J* = 7.70 Hz, 4H, 3,5-pyridinium), 9.01 (d, *J* = 9.90 Hz, 8H, pyrrole), 8.27 (d, *J* = 8.41 Hz, 4H, 2,6-phenyl), 6.96 (d, *J* = 5.55 Hz, 4H, 3,5-phenyl), 4.72 (s, 6H, N<sup>+</sup>-Me), 2.56 (s, 4H, -CH<sub>2</sub>), 1.29 (d, *J* = 7.71 Hz, 6H, -CH<sub>3</sub>), -2.89 (s, 2H, NH). Anal. calcd for C<sub>50</sub>H<sub>42</sub>N<sub>6</sub>I<sub>2</sub>O<sub>4</sub>·H<sub>2</sub>O: C, 56.51; H, 4.17; N, 7.91. Found: C, 55.24; H, 4.25; N, 8.17. ES-MS EtOH, *m/z*: 790 (M<sup>+</sup>), 395 (M<sup>2+</sup>). UV-Vis (10 μM in Tris buffer), λ<sub>max</sub> (nm) (log ε): 422(5.01), 520(3.91), 561(3.72), 582(3.41), 644(3.28).

**5-(4-Methoxyphenyl)-10,15,20-tri(1-methylpyridinium-4-yl)porphyrin (4).** Similar method as 1 was employed to synthesize 4, with 4-pyridinecarboxaldehyde was replaced by 0.7 mL (0.01 mol) 4-pyridinecarboxaldehyde and 3.6 g (0.03 mol) *p*-hydroxybenzaldehyde, and the eluent was replaced by CH<sub>2</sub>Cl<sub>2</sub>/EtOH = 15 : 1. The purple powder obtained from the third band was then methylated by an excess amount of methyl iodide afforded target compounds. Yield: 92.7%. The spectroscopic results obtained from: <sup>1</sup>H NMR (500 MHz, DMSO): chemical shift δ: 9.33 (d, *J* = 7.75 Hz, 2H, 2,6-pyridinium), 9.04 (d, *J* = 7.70 Hz, 2H, 3,5-pyridinium), 9.01 (d, *J* = 9.90 Hz, 4H, β-pyrrole), 8.80 (d, *J* = 9.90 Hz, 4H, β-pyrrole) 8.76 (d, *J* = 9.90 Hz, 4H, β-pyrrole), 8.30 (d, *J* = 8.41 Hz, 4H, 2,6-phenyl), 6.96 (d, *J* = 5.55 Hz, 4H, 3,5-phenyl), 4.72 (s, 6H, N<sup>+</sup>-Me), 2.56 (s, 6H, -CH<sub>2</sub>), 1.26 (d, *J* = 7.71 Hz, 9H, -CH<sub>3</sub>), -2.88 (s, 2H, NH). Anal. calcd for C<sub>53</sub>H<sub>44</sub>N<sub>5</sub>I<sub>3</sub>O<sub>6</sub>·H<sub>2</sub>O: C, 64.18; H, 4.67; N, 7.06. Found: C, 65.33; H, 4.75; N, 7.18. ES-MS EtOH, *m/z*: 846 (M<sup>+</sup>). UV-Vis (10 μM in Tris buffer), λ<sub>max</sub> (nm) (log ε): 424(5.01), 521(3.97), 558(3.72), 582(3.41), 646(3.21).

The <sup>1</sup>H NMR spectra of these compounds are given as ESI in Fig. S1.†

For the hemolysis testing experiment, 4 mL fresh anti-coagulation human blood was diluted with 5 mL physiological saline. 1 mL SPION-COOH nano suspension (concentration is 1.0 mg mL<sup>-1</sup>, drug free) was incubated in the 37 °C water bath for 30 min, and then 1 mL diluted blood was added to the nano suspensions, following by shocking for 60 min in the water bath. The mixture was then centrifuged at 1000 × *g* centrifugal for 5 min, and the absorbance of the supernatant at 545 nm was measured. Physiological saline and distilled water were used as negative control and positive control, respectively.

The hemolysis rates of materials were calculated using the following equation:

$$H\% = \frac{A_m - A_n}{A_p - A_n} \times 100\%$$

Here, *H*% refers to the hemolysis rates of materials, *A<sub>m</sub>* refers to the absorbance of the supernatant for the studied material

at 545 nm,  $A_n$  refers to the absorbance of the supernatant for the negative control at 545 nm,  $A_p$  refers to the absorbance of the supernatant for the positive control at 545 nm.

To investigate the biocompatibility of the SPION-COOH, human umbilical vein endothelial (HUVE) and HeLa cells were placed in 96-well plates at a cell density of  $1 \times 10^5$  cells per well. After incubation for 24 h, the medium was replaced with SPION-COOH nanosphere solutions (dissolved in fresh medium) at different concentrations. After incubation for a further 48 h, standard MTT assay was carried out to determine the cell viabilities relative to the control untreated cells.

### The adsorption and release of porphyrin@SPION

The schematic diagram of loading cationic porphyrins to SPION was given in Fig. 2. Porphyrin@SPION nanospheres were obtained by incubating the porphyrins with the SPION-COOH PBS buffer at pH 7.40 and gently shaking for 24 h, the drug-loaded SPION were harvested by centrifugation. Finally, the nanoparticles were washed with the mixture of cold ethanol and dichloromethane (1 : 1) to remove the residual porphyrins and used immediately afterwards. The porphyrin concentration in the supernatant was measured by means of UV-vis spectrophotometry, using a calibration curve established previously. The porphyrin loading (%) was defined as thus obtained by method of subtractive using loading porphyrin vs. SPION (w/w). Each determination was performed in quadruplicate. The SPION nanospheres loading porphyrins 1, 2, 3 and 4 were named as porphyrin 1@SPION, porphyrin 2@SPION, porphyrin 3@SPION, porphyrin 4@SPION, respectively.

To start the drug release, small aliquots of the drug loaded porphyrin@SPION nanospheres were added to equal volumes of PBS buffer pH 5.86 or 7.40, thermostated at 37 °C and continuously shaken. At given time intervals, each tube was centrifuged, and the released drug concentration in the supernatant was determined from the intensity of the drug absorption. The release ratio was calculated from the porphyrin in the solution vs. the original porphyrin loaded on the nanospheres (w/w).

### Prussian blue staining

HeLa cells ( $1 \times 10^5$ ) were seeded on 24-well plates and incubated overnight at 37 °C with 5% CO<sub>2</sub> in a humidified chamber. A solution of the magnetic nanospheres with a concentration of 0.1 mg mL<sup>-1</sup> was then added and the cells were cultured for 4 h. After the end of the culture period, each well was washed three times with phosphate buffered saline (PBS), treated with 4% paraformaldehyde solution at 4 °C for 30 min to fix the cells, and washed three times with PBS again. A 1 : 1 mixture of 5% potassium ferrocyanide(II) trihydrate solution and 5% HCl was added to each well and the cells were incubated at room temperature for 1 h before being counterstained with neutral red. Each well was then washed three times with PBS and the cells were immediately examined and analyzed by light microscopy.

### ICP-MS

To quantitatively measure the cellular uptake of the nanospheres, HeLa cells were seeded in 10 cm tissue culture dishes

and incubated for 24 h. The medium was removed and replaced with fresh medium containing the 0.1 mg mL<sup>-1</sup> porphyrin 3@SPION. After 4 h incubation, the cells were washed with PBS, trypsinized, and collected. The cells were counted and digested with HNO<sub>3</sub> (65%, 0.5 mL).

### Magnetic targeting study

HeLa cells were seeded in a 60 mm Petri dish and incubated overnight, and then a solution of the magnetic nanospheres with a concentration of 0.1 mg mL<sup>-1</sup> was added. For magnetic targeting study, a magnet (about 4 T) was placed beside the Petri dish. After incubation for 24 h, the Petri dish was photographed and the cells in the position of magnet (targeting area) and the area with a much weaker magnetic field strength (control area) were observed using a light microscope. For photodynamic combination therapy, after incubated nanospheres with cells for 12 h, the plates were irradiated with UV-A (310–390 nm, 4 mW) or visible (400–800 nm, 2 mW) light for 10 min. Then the wells were incubated for another 12 h and treated with the same procedure as described above.

### Detection of singlet oxygen

Singlet oxygen in aqueous was determined following the Kraljić procedure.<sup>29</sup> Solution of *p*-nitrosodimethylaniline (RNO, 30 μM) and imidazole (0.5 mM) in PBS (10 mM, pH = 5.86 or 7.40) was added into porphyrin@SPION (0.1 mg mL<sup>-1</sup>) and then irradiated with visible (400–800 nm, 2 mW) light. The absorbance spectra of the solution were recorded at 30 s intervals.

BEL-7402 cells were seeded into six-well plates and incubated for 24 h. The cells were cultured in RPMI 1640 supplemented with 10% of fetal bovine serum (FBS) and incubated at 37 °C and 5% CO<sub>2</sub>. The medium was removed and replaced with medium containing porphyrin@SPION nanospheres (0.1 mg mL<sup>-1</sup>) for 24 h. The cells were washed with RPMI 1640 medium and then incubated with 10 μM DCFH-DA in RPMI 1640 medium at 37 °C for 20 min. After washing twice with RPMI 1640 medium, cells were irradiated with 660 nm LED light for 5 min. The cells were then harvested and the cell pellets were suspended in PBS-EDTA, which were then imaged by fluorescence microscope. The fluorescence intensity was determined by microplate analyzer (Infinite M200, TECAN, Switzerland) with excitation at 488 nm and emission at 525 nm. The fluorescence intensity was calculated by the determined fluorescence intensity minus the fluorescence intensity of the complexes in the corresponding concentrations of porphyrin@SPION nanospheres.

### Cell cytotoxicity

Cell viability is measured by WST assay to evaluate the effects of porphyrin@SPION-initiated photodynamic therapy. The HeLa cells were seeded for 48 h in standard 96-well plates at 37 °C in a 5% CO<sub>2</sub>/95% air humidified incubator. The cells were collected and re-suspended in PBS buffer (at  $1 \times 10^5$  cells per well), then seeded in 96-well plates (well diameter: 6.4 mm) to attach for 24 hours before treatment with porphyrin@SPION. The medium at pH 5.86 was prepared from commercially

available RPMI 1640 medium of pH 7.4 by addition of an appropriate amount of HCl (0.2 M). Porphyrin@SPION was added to pH 7.40 or pH 5.86 medium (containing 0.5% DMF) to produce a final concentration of 0.1 mg mL<sup>-1</sup>. The above porphyrin@SPION solution was then subjected to vortex or sonication or a combination of both. A solution (10.00 μL) of porphyrin@SPION or free porphyrins at the same concentration was added to the HeLa cells. The mixture was then exposed to visible simulated solar light for 20 minutes irradiated with UV-A (310–390 nm, 4 mW) or visible (400–800 nm, 2 mW) light for WST tests. To perform WST assay, WST kit was added to each well and incubated for 30 minutes. The cells were centrifuged, and the suspension was discarded. The absorbance was read at 450 nm using a Multiskan Ascent Plate Reader. The IC<sub>50</sub> indicates the concentration of free porphyrins or porphyrins in the nanospheres.

### Statistical analysis

All of the data were expressed as the mean ± SD. Differences between two groups were analyzed by a two-tailed Student's *t* test. Differences with \**P* < 0.05 were considered statistically significant.

### Fluorescence microscopy of apoptosis assays

Forty eight hours after exposure to porphyrin@SPION nanospheres, the cancer cells were washed twice with phosphate buffer solution, and were then stained with 0.01 mg mL<sup>-1</sup> Hoechst 33258 staining solution at 37 °C for 30 min according to the manufacturer's instructions. Finally, the cells were observed under a fluorescence microscope.

HeLa cells in the logarithmic growth phase were seeded in 24-well plates and allowed to attach overnight. Cells were incubated with 0.1 mg mL<sup>-1</sup> porphyrin 3@SPION nanospheres for 12 h under dark or exposed to 660 nm light for 5 min, then stained with an annexin V-FITC apoptosis detection kit (Beyotime Institute of Biotechnology, China) as described in the manufacturer's instructions, and observed by fluorescence microscopy.

### Spectral experiments

The absorption and fluorescence titrations were carried out by the stepwise addition of porphyrin@SPION solution to a cell containing 10 μM HSA solutions. After preparation, the reaction systems were incubated for 5 min at room temperature before measurement. Synchronous fluorescence spectra were obtained by using synchronous excitation and emission scanning with right-angle geometry. The reaction solutions for CD spectral experiments were placed in a 0.1 cm path length cell, and each spectrum was the average of three scans.

### Molecular model

In order to find out the exact binding mode of porphyrins to HSA, we perform docking simulations based on the AutoDock program (downloaded from the <http://autodock.scripps.edu/>) and DS Visualizer software. The three-dimensional structural

information of protein from [http://www.rcsb.org/pdb/\(ID:1AO6\)](http://www.rcsb.org/pdb/(ID:1AO6)). The 3D structure of daunomycin was generated in Discovery Studio 4.5 Client. The grid center coordinates of box along the *x*-, *y*-, *z*-axes are set to 126 Å, 126 Å and 126 Å. The Lamarckian genetic algorithm is employed to search the docking conformation.

## Results and discussion

### Characterization and drug release of porphyrin@SPION nanospheres

**Characterization.** All the porphyrin@SPION nanospheres have the similar morphology and porphyrin 1@SPION was taken as an example to characterize these nanospheres. SEM image of the porphyrin 1@SPION given in Fig. 3a exhibit the uniform roughly spherical shape of these nanospheres. TEM image in Fig. 3b clearly shows that the SPION core is well embodied in the particle.

The chemical composition of the organic layers, namely the presence of the porphyrins, was confirmed by solid state UV-Vis spectra. Fig. 3c exhibits the solid-state UV-Vis spectra of SPION and porphyrin 1@SPION, and the UV-Vis spectra for porphyrin 1 was given as inserted. It found that SPION has no substantial absorption while the porphyrin 1@SPION has the characteristic absorption peak (Soret band around 420 nm) of porphyrin. Meanwhile, the FTIR spectra (Fig. S2 in ESI<sup>†</sup>) also confirmed the existing of the porphyrins on the nanospheres. It is found that compared with that of pure SPION, the intensity of the pyrrole ring's vibration bands at 887 cm<sup>-1</sup> and 1446 cm<sup>-1</sup>, which are the characteristic FTIR signals of porphyrin, increases remarkably. Moreover, thermostability of the porphyrin@SPION was tested and further proves the existence of SPION and porphyrin, with two degrade degrees at 274 °C for organic shell and 488 °C for inorganic core, and respectively. These results evidenced the successful loading of porphyrins on SPION nanospheres.

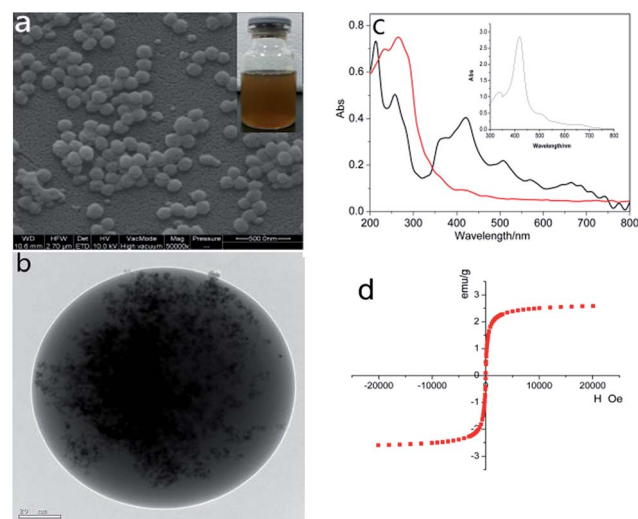


Fig. 3 The characterization of cationic porphyrin 1@SPION nanospheres: SEM image (a), TEM image (b), solid UV-Vis spectra of porphyrin (insert), SPION (—) and porphyrin@SPION (—) (c) and magnetic hysteresis loop (d).

Porphyrin@SPION nanospheres are superparamagnetic and have excellent magnetic responsibility, which is the key factor for their targeting. Magnetic hysteresis loop (Fig. 3d) shows that magnetic nanospheres porphyrin 1@SPION exhibit superparamagnetic behavior with zero coercivity and remanence. The saturation magnetizations of these magnetic nanospheres are almost the same, about  $2.75 \text{ emu g}^{-1}$ , which is lower than that of SPION nanoparticles. It could be explained by the porphyrins coating of the SPION nanoparticles in nanospheres.<sup>19–21</sup> It was experimentally observed that these nanospheres dispersed in water were rapidly attracted by a conventional magnet placed close to the reaction vessel (Fig. S4†), further demonstrating the efficacy of magnetic separation.

The hemolysis rate for the SPION-COOH nanospheres is 0.51%, which is far lower than the maximum hemolysis rate (5%) for the medical device requested by FDA. This result suggests that the studied material is biocompatible for the circulating blood.

Meanwhile, it is well known that the cell toxicity is a very important part for the biocompatibility of the nanoparticles. To more deeply assess the toxicity of SPION-COOH nanospheres (drug-free), two different cell lines, human umbilical vein endothelial (HUVE) cells and HeLa cells were employed and incubated with nanospheres for 48 h. The cell viability of these cell lines with nanospheres at concentrations ranging from 0.03 to  $1.0 \text{ mg mL}^{-1}$  was given in Fig. 4.

From Fig. 4, it is found that no appreciable deduction in cell viabilities were observed, indicating that the SPION-COOH nanospheres are highly biocompatible for HeLa and HUVE cells.

**Drug loading and release.** To optimize the protocols of porphyrin loading on the ferrofluids, we studied loading efficiencies of these porphyrins to the SPION-COOH surface during incubation at pH 7.40 (Fig. 5a). The loading process of these porphyrins reaches equilibrium in less than 2 h. Meanwhile, for initial drug/SPION (w/w) ratio at 0.05, the extents of porphyrin loading reach up to 36.9%, 30.2%, 21.5% and 12.4% for porphyrins 1, 2, 3 and 4, respectively. As far as we know, these drug loading exceed the maximal loading values for porphyrins reported before.<sup>13</sup> Thus, the proposed novel method in this work was proved to be particularly efficient. It is notable that more positive charges are favored by the loading process, indicating that the electrostatic interaction is the main driving force for the adsorption.

The *in vitro* release of porphyrins from loaded SPION ferrofluids was studied in Tris buffer pH 7.40 (pH of blood plasma)

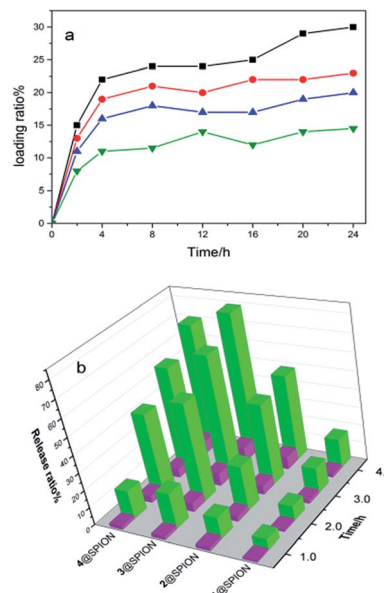


Fig. 5 (a) *In vitro* porphyrin 1 (■), 2 (●), 3 (▲), 4 (▼) loading on SPION-COOH vs. time; (b) release of porphyrins from porphyrin@SPION at pH 5.86 (■), 7.40 (■) (37 °C).

and 5.86 (pH of tumor cells) at 37 °C, respectively. The releases were monitored with UV and the release ratio results were given in Fig. 5b. From Fig. 5b, one can easily find that the tumor cell condition (pH 5.86) is much more favored by all the nanospheres than the blood plasma condition (pH 7.40). When considering the porphyrin 3@SPION as an example, at pH 5.86, the drug released continuously during 4 h then reaches a plateau equivalent to ~78% from the loaded drug. However, the release at pH 7.40 is relatively slow and sustained, with only about 8% of original porphyrin releases from porphyrin 3@SPION when achieving the equilibrium. This indicates that porphyrin@SPION has smart pH-controlled release and potential pH targeting to tumor cells. The observed pH sensitivity is hypothesized to facilitate drug release from SPION once inside the acidic endosomal compartment and increase the intracellular bioavailability of the drug.<sup>22</sup>

Meanwhile, Fig. 5b also shows that the release ratio for the porphyrins from porphyrin@SPION follows the order of  $3 > 4 > 2 > 1$ . Generally, less positive charges on the porphyrin molecules are more favored by the release process. This result could be best understood by the fact that higher positively charged porphyrins have stronger electronic attraction with the modified SPION surface and thus are more difficult to release into the solution. It is interesting that the result for porphyrins 3 and 4 is somewhat controversial to the conclusion above, with dicationic porphyrin 3 releasing more efficiently than monocationic porphyrin 4. This could be mainly attributed to the different molecular solubility in the solution. Porphyrin 3 with two positive charges is more soluble than monocationic porphyrin 4 in the release buffer. Positive charge(s) on the porphyrin molecule seems to be a double-edged sword in loading and release processes, and dicationic porphyrin 3 is more favored than other studied porphyrins in this research.

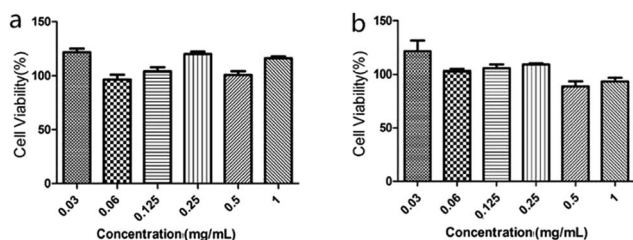


Fig. 4 HeLa (a) and HUVE (b) cell viability under different concentrations of SPION-COOH nanospheres.

## Magnetic targeting and cell cytotoxicity research

**Cellular uptake.** It is well accepted that the biochemical processes that control the complexity of life occur in the cell cytosol and different subcellular organelles. Thus, the cellular uptake efficiency of the magnetic nanospheres was evaluated in order to assess its potential for efficient delivery of drug molecules into cells.<sup>23,24</sup>

The presence of the magnetic nanospheres in HeLa cells was detected through determining the intracellular "Fe" in HeLa cells, which had been incubated with the magnetic nanospheres by Prussian blue staining method. Since porphyrin 3@SPION exhibits the smartest pH release ability, it is chosen as the model to elucidate the cellular uptake, as well as the anticancer mechanism research. In the absence of porphyrin 3@SPION nanospheres, we did not observe any blue staining of the control cells (Fig. 6a). However, as shown in Fig. 6b, after the incubation with the porphyrin 3@SPION nanospheres, substantial blue spots were observed in most of the cells. The majority of the blue spots are localized around the cell membrane and throughout the cytoplasm, indicating high cellular uptake of the magnetic nanospheres.<sup>24,25</sup>

Moreover, the intracellular Fe content can be easily and precisely determined by ICP-MS. After incubation of HeLa cells with porphyrin 3@SPION nanospheres for 4 h, the cells were harvested and digested and the intracellular Fe contents were determined to be 73 ng/10<sup>6</sup> cells by ICP-MS.

**Magnetic targeting study.** An magnetic targeting experiment was carried out to examine the magnetic targeting property of the magnetic nanospheres *in vitro*. A magnet (about 4 T) was placed beside the Petri dish, and the cells incubated with porphyrin 3@SPION in two locations, which referred to as the targeting area (red circle) and the control area (blue circle), were photographed and compared (Fig. 7). Red circle points to the position closest to the magnet and thus is in the strongest magnetic field, while the magnetic field applied to blue circle is much weaker.

As shown in Fig. 7, after incubation under UV-A or Vis light, clear morphological changes were observed for the cells in red circles. Most of the adhered HeLa cells appeared to be round and bright, with floating in the cell culture media. This is the significant signal of cell death. It is found that Vis light leads to more cell death in the magnetic field. However, under incubation in the dark, the morphology of the HeLa cell changed negligibly. This observation clearly proved the photodynamic potential of the porphyrin@SPION nanospheres.

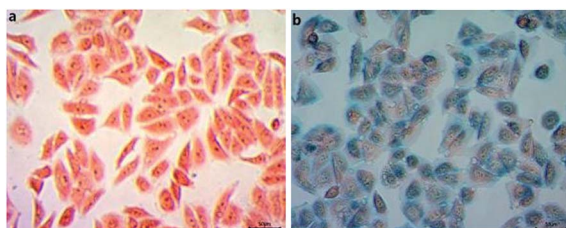


Fig. 6 Prussian blue staining of HeLa cells treated in the absence (a) and presence the porphyrin 3@SPION (b) magnetic nanosphere (0.1 mg mL<sup>-1</sup>) for 4 h.

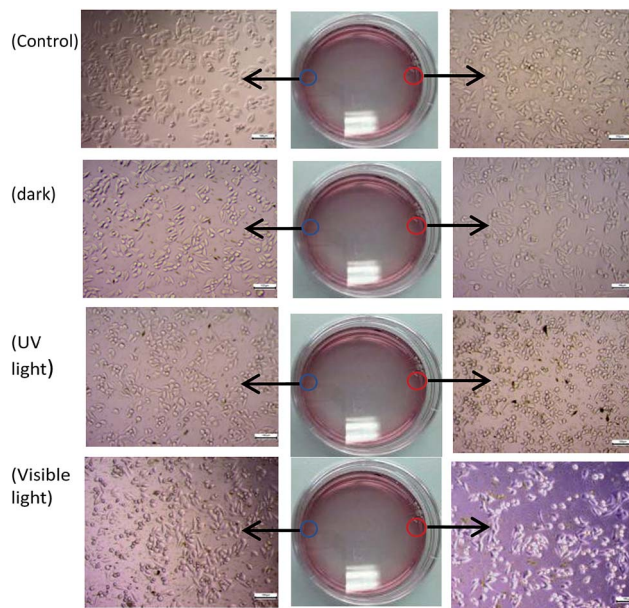


Fig. 7 Optical micrographs of HeLa cells at the targeting area (red circle) and the control area (blue circle) after incubating with the magnetic nanospheres (0.1 mg mL<sup>-1</sup>) under dark, UV-A and visible light at pH 5.86.

Compared with the large change in the magnetic region, the cells in the weak magnetic region (blue circle) suffered much fewer death than the magnetic position. The majority of the cells remained their long shape and uniform morphology, under dark or irradiation. This indicates that the magnetic nanospheres could efficiently accumulate to the targeted area under a magnetic guidance. The results here allowed the conclusion that these porphyrin@SPION nanospheres have photodynamic and magnetic targeting multifunction.

## Induction of apoptosis as evidenced by Hoechst 33258

Since live/dead cell staining was used to visualize the cell viability more directly by fluorescence microscope after different treatments, we identified the cell change in the presence of porphyrin@SPION by Hoechst 33258 staining.

Fig. 8 shows representative Hoechst 33258 fluorescence photomicrographs of cultured HeLa cells treated with porphyrin 3@SPION under dark, UV-A or visible light. In control cultures (Fig. 8a), nuclei of HeLa cells appeared with regular contours and were round and large. Under dark, the cells have no significant change. By contrast, the condensation of nuclei characteristic of apoptotic cells was evident. Most nuclei of HeLa cells treated under UV-A or visible light appeared hypercondensed (brightly stained), and the typical apoptotic bodies were observed, which was different from what was observed in the control cells. This may imply that these nanospheres can cause proliferative suppression of cancer cells *via* the induction of apoptosis. Further investigations are required to fully understand the mechanism involved in the induction of apoptosis by the nanospheres.

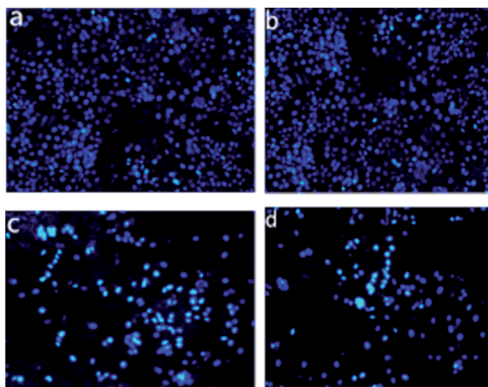


Fig. 8 Effects of porphyrin 3@SPION on the morphology of HeLa cells were assayed by Hoechst 33258 staining with fluorescence microscopy (original magnification 400 $\times$ ): control (a) and incubation in the dark (b), UV-A (c) and visible light (d) for 48 h at pH 5.86.

### Annexin V–FITC apoptosis detection

It is widely accepted that the loss of plasma-membrane asymmetry and attachment is one of the striking morphological features of the apoptotic process. In apoptotic cells, the membrane phospholipid phosphatidylserine (PS) is translocated from the interior to the exterior of the plasma membrane, thereby exposing PS to the external cellular environment. Annexin V is a protein that has a high affinity for PS and thus could bind to cells with exposed PS. By conjugating with fluorochromes including fluorescein isothiocyanate (FITC), Annexin V can serve as a sensitive fluorescent probe for fluorescence-microscopy analysis of cells that are undergoing apoptosis.

FITC–annexin V staining precedes the loss of membrane integrity that accompanies the last stages of cell death resulting from either apoptotic or necrotic processes. Therefore, staining with FITC–annexin V is typically used in conjunction with a nuclear dye such as propidium iodide (PI) to identify early apoptotic cells. Viable and early-apoptotic cells with intact membranes exclude PI, whereas the membranes of dead and late-apoptotic cells are permeable to PI, and thus the nucleus can be labeled.

We studied the mode of cell death induced by porphyrin 3@SPION nanospheres by fluorescence staining with an FITC–annexin V apoptosis detection kit for the morphological assessment of cell apoptosis. The cytological changes were classified into three types: (1) viable cells are FITC–annexin V and PI negative; (2) cells that are in early apoptosis are FITC–annexin V positive and PI negative; and (3) cells that are in late apoptosis or already dead are both FITC–annexin V and PI positive. From Fig. 9a, no obvious fluorescence was observed in the control cells. Meanwhile, there were negligible fluorescent signals when HeLa cells treated with porphyrin 3@SPION nanospheres under dark (Fig. 9b). However, after exposed to the light, HeLa cells treated with porphyrin 3@SPION exhibited significant morphological changes. We can find from Fig. 9c that, the cell membranes of all of the treated cells were FITC–annexin V positive (green fluorescence) but no PI signal was

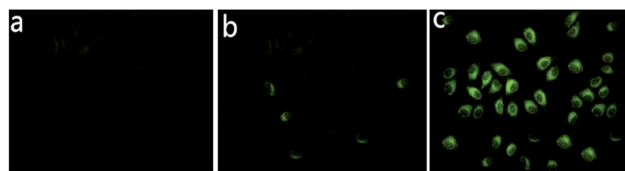


Fig. 9 (a) Annexin V–FITC apoptosis detection Fluorescence microscopy images of HeLa cells treated with control cell media; (b) HeLa cells treated with porphyrin 3@SPION under dark; (c) HeLa cells treated with porphyrin 3@SPION under dark for 12 h and then irradiated by 660 nm light for 5 min.

detected in the nucleus, indicating that the HeLa cells underwent early apoptosis induced by porphyrin 3@SPION nanospheres.

### Reactive oxygen species studies

The role played by ROS in apoptosis is becoming increasingly recognized. It is widely accepted that porphyrins induce apoptosis through ROS generation.<sup>6,7</sup> ROS levels of these porphyrin@SPION nanospheres were investigated with a fluorescence microscope and microplate analyzer using H<sub>2</sub>DCFDA as a probe. H<sub>2</sub>DCFDA is a fluorescent dye that diffuses through cell membranes and is hydrolyzed by intracellular esterases to DCFH. In the presence of ROS, DCFH could be oxidized to DCF, whose fluorescent level corresponds to the level of generated ROS. Fluorescent images and intensities were given in Fig. 10.

As shown in Fig. 10, in the control (a), no fluorescent spots are found. After BEL-7402 cells were incubated with 0.1 mg mL<sup>-1</sup> porphyrin 3@SPION nanospheres for 24 h without irradiation, negligible fluorescent spots were observed (Fig. 10b). However, after irradiation at 660 nm for 5 min, clear fluorescence can be observed under a fluorescence microscope (Fig. 10c). To determine quantitatively the fluorescence intensity of DCF, the ROS levels were also evaluated by with microplate analyzer. The results indicated that the mean fluorescence intensity (MFI) of the cells treated with porphyrin 3@SPION under light irradiation is almost 5-times higher than that obtained in the dark (Fig. 10d). It is well known that these highly toxic ROS could damage the cellular proteins, lipids and nucleic acids. Therefore, elevated intracellular ROS level causes oxidative stress and a series of signal transduction pathway changes, which are highly related to transcription factors, cell cycle regulation, inflammation, and so on. The cellular metabolism changes following PDT treatment make the cells more fragile to chemotherapeutic treatment and result in apoptosis or necrosis.

### The <sup>1</sup>O<sub>2</sub> production of the porphyrin@SPION nanospheres

The object of this research is to further understand the mechanism of the photodynamic cell cytotoxicity of the porphyrin@SPION nanospheres. The basic principle of PDT is the generation of highly cytotoxic ROS, especially singlet oxygen (<sup>1</sup>O<sub>2</sub>), under light activation. The capacity of porphyrin 3@SPION to generate <sup>1</sup>O<sub>2</sub> in aqueous solution under UV-A or visible light at pH 5.86 or 7.40 was comparatively assessed

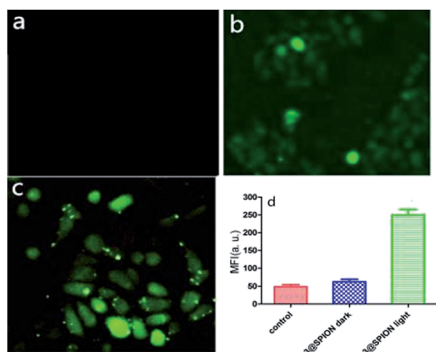


Fig. 10 Fluorescent images of BEL-7402 cells alone (a) and BEL-7402 cells with  $0.1 \text{ mg mL}^{-1}$  porphyrin 3@SPION in the dark (b) or irradiated with 660 nm light (c). (d) gives the fluorescent intensity values for the images.

following the Kraljić procedure. Fig. 11 gives the absorption change of RNO in the presence of porphyrin 3@SPION under visible light irradiation. The absorbance of RNO at 440 nm decreased remarkably owing to the photooxidation bleaching effect after irradiation for 180 s with porphyrin 3@SPION, which indicated the significant production of  $^1\text{O}_2$  from porphyrin 3@SPION when exposed to visible light.

The  $^1\text{O}_2$  production at pH 5.86 was observed higher than that at pH 7.40 under UV-A or visible irradiation. This could be explained by the fact that, at an acidic solution, the attached porphyrin molecules could be separated from the surface of the SPION-COOH nanoparticles because the surface charge became less negative *via* the protonation of carboxyl groups with decreasing pH value. Since molecular aggregation is assumed to be absent or minimized with cationic porphyrins in the solution,<sup>26</sup> the increased release of porphyrins leads to enhanced singlet oxygen generation, thus an improvement in cell apoptosis under visible light in the magnetic targeting study above. This result is highly consistent with our conclusion on the  $^1\text{O}_2$  PDT mechanism of cationic porphyrins before.<sup>27</sup> These features make SPION-attached cationic porphyrin a promising candidate for use in PDT for cancer treatment in which efficient  $^1\text{O}_2$  production at acidic pH and sensitizer deactivation at

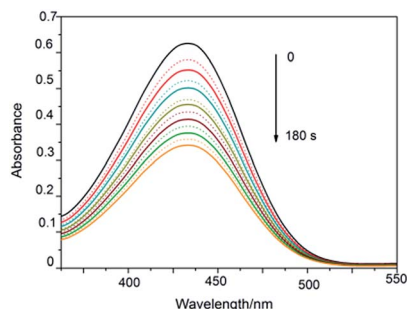


Fig. 11 Singlet oxygen detection by photooxidation of RNO under light irradiation. To the solution of *p*-nitrosodimethylaniline (RNO,  $30 \mu\text{M}$ ), imidazole ( $0.5 \text{ mM}$ ) in PBS ( $10 \text{ mM}$ ,  $\text{pH} = 7.4$ ) was added to porphyrin 3@SPION, then the solution was irradiated with visible light at pH 5.86 (solid lines) or 7.40 (dot lines) for different periods of time.

physiological pH are desirable. This pH-triggered therapeutic selectivity was further confirmed by WST cell cytotoxicity tests.

### Cell cytotoxicity research

It has been demonstrated previously that drug-free SPION produce negligible cytotoxicity on cancer cells.<sup>28</sup> The  $\text{IC}_{50}$  values for the porphyrins and corresponding porphyrin@SPION nanospheres are given in Table 1.

From Table 1, porphyrin 1 (TMPyP), which is a well-known anticancer research model, exhibits the best cell phototoxicity under both UV and Vis light. However, because of its poor release which further leads to a low  $^1\text{O}_2$  production, porphyrin 1@SPION has weak antitumor ability, with  $\text{IC}_{50}$  values reach up to  $27.3 \mu\text{M}$  and  $47.2 \mu\text{M}$  under Vis light at pH 5.86 and 7.40, respectively. Porphyrin 4@SPION also has low anticancer efficiency, which may result from the high  $\text{IC}_{50}$  value of porphyrin 4 itself as well as its low release efficiency. However, porphyrin 3@SPION could efficiently inhibit the HeLa cells under both UV and Vis light. It seems that the anticancer ability for porphyrin@SPION controlled the synergy of two factors: the  $\text{IC}_{50}$  of porphyrin molecule itself and release efficiency of porphyrin from the SPION surface. Both lower  $\text{IC}_{50}$  and higher release efficiency are important for porphyrin@SPION nanospheres. For porphyrin molecules, lower  $\text{IC}_{50}$  always related to higher positive charges, which are however disfavored by the release process. Dicationic porphyrin 3 has a good equilibrium between these two factors has thus porphyrin 3@SPION has a relative high anticancer efficiency.

However, it is notable that it is impossible to put all the porphyrin@SPION nanospheres into the well that were internalized by the cell or all the porphyrin released completely from the nanospheres. The major mechanism of action of free porphyrin is an intercalation in the DNA and an inhibition of the topoisomerase II.<sup>8–10,29</sup> This hypothesis does not exclude the participation of other supplementary mechanisms of action. To further explore the mechanisms of this, more efforts are currently undergoing.

### Probing the interaction of porphyrin@SPION with HSA

Numerous exogenous and endogenous drugs were carried by human serum albumins (HSA) when they are delivered in the blood plasma of human body. It is understandable that the significant changes at secondary structure of HSA is a hallmark of the drug bio-safety in the delivery process. The object of following research is to elucidate the HSA binding behaviors and mechanism of these porphyrin@SPION, which could be used to evaluate the delivery bio-safety of these nanospheres.

### Absorption spectroscopy

The structural changes of proteins are often explored using by the UV-visible absorption spectroscopy.<sup>30</sup> Fig. 12 exhibits the UV-visible absorption of HSA in the presence of porphyrin 3@SPION.

As Fig. 12 shows, the characteristic peak at 198 nm, which could be mainly attributed to the peptide bonds in the protein and reflects the framework conformation of HSA, has no

Table 1 (Photo)cytotoxicity of the porphyrins and porphyrin@SPION towards HeLa cells

	IC <sub>50</sub> (μM)							
	1@SPION (1)		2@SPION (2)		3@SPION (3)		4@SPION (4)	
pH	5.86	7.40	5.86	7.40	5.86	7.40	5.86	7.40
Dark	>100							
UV-A	25.2 ± 2.8 (1.2 ± 0.3)	43.1 ± 3.7 (1.5 ± 0.4)	19.3 ± 1.7 (3.2 ± 0.8)	35.2 ± 4.8 (5.5 ± 0.4)	13.5 ± 1.1 (5.7 ± 0.6)	26.2 ± 1.8 (1.5 ± 0.4)	24.5 ± 1.6 (11.5 ± 1.1)	37.2 ± 2.6 (14.5 ± 0.9)
Visible	27.3 ± 2.1 (0.7 ± 0.2)	47.4 ± 4.1 (0.9 ± 0.2)	16.8 ± 1.4 (2.8 ± 0.6)	37.3 ± 5.1 (4.9 ± 0.2)	12.7 ± 1.0 (5.4 ± 0.3)	28.3 ± 2.1 (0.9 ± 0.2)	28.2 ± 2.3 (10.2 ± 2.3)	39.5 ± 3.2 (12.9 ± 1.2)

significant change with the gradual addition of porphyrin@SPION. Meanwhile, with the increase of porphyrin@SPION solution, the absorption at 280 nm, which is the characteristic absorption peak of the aromatic ring amino acids, has no obvious change (see Fig. 12 inserted). Since it is widely accepted that the enhancement around 280 nm is the signal of unfolding the skeletal structure of HSA, the negligible change at this region, as well the non-obvious change at 198 nm, indicate the structure of HSA is not affected with the addition of porphyrin@SPION.<sup>31</sup>

### Fluorescence quenching

The fluorescence emission of HSA in the presence of porphyrin@SPION was monitored to further reveal the interaction between these nanospheres and protein. As is shown in Fig. 13, the fluorescence intensity decreased slightly with the titration of porphyrin 3@SPION, indicating that the drug delivery alters the spatial structure of HSA and leads to a less hydrophobic environment the fluorescence chromophore placed.<sup>32–34</sup> The newly appeared shoulder peak located at 310 nm could be attributed to the new state of porphyrin@SPION bound HSA.<sup>35</sup> This new state represents efficient binding of drugs with HSA, which is very significant for the drug delivery by the protein.

Stern–Volmer equation is widely employed to analyze the quenching mechanism:<sup>36</sup>

$$F_0/F = 1 + K_q \zeta_0 Q = 1 + K_{sv} Q \quad (1)$$

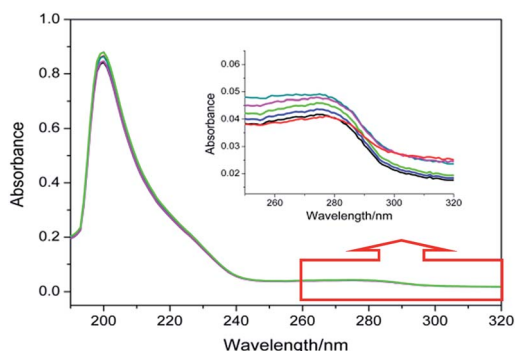


Fig. 12 Absorption spectra of HSA with different concentration of porphyrin@SPION in PBS solution. Insert: the absorption change from 260 nm to 320 nm. Conditions: HSA:  $1 \times 10^{-6}$  mol L<sup>-1</sup>; porphyrin@SPION: 0 (—); 2 (—); 4 (—); 6 (—); 8 (—); 10 (—)  $\times 10^{-4}$  mg mL<sup>-1</sup> (pH = 7.40).

where  $F$  and  $F_0$  are the fluorescence intensities in the presence and absence of a quencher, respectively.  $K_{sv}$ ,  $K_q$ ,  $\zeta_0$  and  $Q$  denote Stern–Volmer constant, quenching rate constant, the original lifetime of HSA ( $10^{-8}$  s)<sup>37</sup> and the concentration of quencher, respectively. The plot of the fluorescence intensity ratio of protein at 340 nm in the absence and presence of quencher as a function of the quencher concentration shows a linear dependence (Fig. S5†). We thus can obtain the bimolecular quenching constants ( $K_q$ ) of the porphyrin 3@SPION is  $3 \times 10^{12}$ , which is much larger than the largest dynamic quenching constant for biological molecules,  $2.0 \times 10^{10}$ .<sup>37</sup> Therefore, we suppose that it is the static rather the dynamic quenching mechanism resulting in the fluorescence quenching of HSA.<sup>37,38</sup>

The binding constant  $K_b$  and binding site number  $n$  can be obtained from the site binding model<sup>39,40</sup> which assumes the existence of  $n$  independent binding sites is expressed in eqn (2):

$$\lg \left[ \frac{F_0 - F}{F} \right] = \lg K_b + n \lg [Q] \quad (2)$$

where  $F$  and  $F_0$  are the fluorescence intensities in the presence and absence of a quencher, respectively. A plot of  $\log(F_0 - F)/F$  versus  $\log Q$  (Fig. 13, insert) yielded the binding constant  $K_b$  as  $1.2 \times 10^3$ . This binding constant is moderate and suitable for the protein delivery of drugs. The binding site number ( $n$ ) is calculated to be 0.91, which is approximately equal to 1, indicating that there is one type of binding site for porphyrin 3@SPION in HSA.

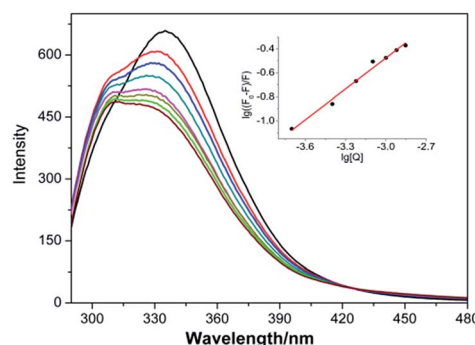


Fig. 13 Fluorescence emission spectra of HSA with different concentration of SPION-DNM in PBS solution. Insert: plot of  $\log(F_0 - F)/F$  versus  $\log Q$ . Conditions: HSA:  $1 \times 10^{-6}$  mol L<sup>-1</sup>; SPION-DNM: 0 (—); 2 (—); 4 (—); 6 (—); 8 (—); 10 (—); 12 (—)  $\times 10^{-4}$  mg mL<sup>-1</sup> (pH = 7.40).

### Synchronous fluorescence spectroscopy

It has been thoroughly emphasized that, the fluorescence of Trp and Tyr residues are highly sensitive to the polarity of its environment, which usually presents a red shift in a more polar surrounding.<sup>41</sup> Thus, the emission shifts of the amino acid residues could be employed to examine the conformational changes of protein. To further probe the binding mechanism of the porphyrin@SPION nanospheres and HSA, synchronous fluorescence spectroscopy experiment was carried out to investigate the conformational changes of protein. The results are shown in Fig. S6,† in which  $\Delta\lambda$  for Trp and Tyr residues are 60 and 15 nm, respectively.

From Fig. S6,† it is apparent that the emission peak had a slight shift, indicating that a less hydrophobic environment of tryptophan residues. The maximum emission wavelength kept its position over the investigated concentration range, which suggests that porphyrin@SPION has negligible effect on the microenvironment of the tyrosine residues. The increasing exposure of amino acid residues is not significant, which is consistent with the conclusion above.

### Circular dichroism spectra

CD spectra of HSA were measured in the absence and presence of porphyrin@SPION to quantitatively ascertain the secondary structure changes of HSA molecules (Fig. 14).

For free HSA, there are two negative bands in the far-UV region at 208 and 222 nm, which are characteristic of  $\alpha$ -helical structure of protein.<sup>42</sup> The  $\alpha$ -helix contents of HSA could be evaluated from the MRE value at 208 nm, using the following eqn (3) and (4):<sup>43</sup>

$$\text{MRE}_{208} = \frac{\text{CD}_{208}}{10C_pnl} \quad (3)$$

$$\alpha\% = \frac{-\text{MRE}_{208} - 4000}{33\,000 - 4000} \quad (4)$$

The  $\alpha$ -helix content of HSA was calculated quantitatively from the eqn (3) and (4). The content of  $\alpha$ -helix changed from

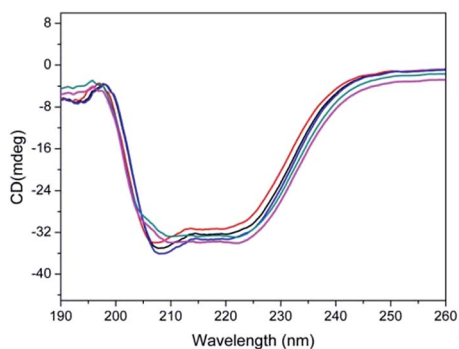


Fig. 14 CD spectra of HSA in the absence (—) and presence of porphyrin 1@SPION (—), porphyrin 2@SPION (—), porphyrin 3@SPION (—), porphyrin 4@SPION (—) in PBS solution. Conditions: HSA 2.5  $\mu\text{M}$ ; porphyrin@SPION:  $2.5 \times 10^{-3}$  mg mL<sup>-1</sup>.

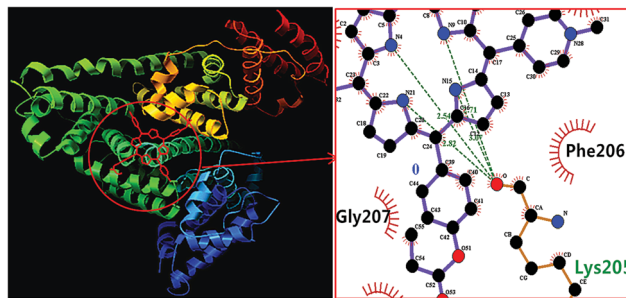


Fig. 15 Docking results of porphyrin and HSA system. Insert: detailed illustration of the binding pocket for porphyrin within 8 Å distance. The hydrogen bonds are marked with green blue lines.

69.48 to 68.75%, 70.12%, 68.24%, 67.95% when porphyrin 1@SPION, porphyrin 2@SPION, porphyrin 3@SPION, porphyrin 4@SPION were added, respectively. It seems that these porphyrin@SPION nanospheres have negligible changes to the secondary structure and undetectable effects on the frame conformation of the HSA. The porphyrin@SPION was thus considered relatively safe in their delivery process, without significant influence to the structure of protein. This result was further evidenced by the theoretical study below.

### Molecular modeling study

AutoDock-based blind docking has been employed to substantiate the spectral experimental results.

As Fig. 15 shows vividly for porphyrin 3 binding with HSA, instead of entering the pocket of HSA structures, porphyrin is bond at the external region of domains, which indicates that the interaction of porphyrin is relatively weak. The chemistry of porphyrin plays a major role in determining the location of bonding site. Moreover, van der Waals interactions also exist, but the hydrogen bonds play a major role in the binding of porphyrin to HSA. The calculation indicates that porphyrin prefers a polar binding site. Thus, compared with the non-specific binding of iron oxide nanoparticles to protein, the interactions of porphyrin@SPION with HSA prefer to occur between porphyrin and protein.<sup>44</sup> The similar HSA binding behaviors of other porphyrins are given in Fig. S7.† The monophyrin will not enter the pocket of HSA structures and is thus safe to the protein.

## Conclusions

In the present contribution, nano-supporting, magnetic effect as well as pH controlling factors were integrated in designing porphyrin@SPION systems in which a series of cationic porphyrins are efficiently loaded on SPION-COOH surface. These pH-controllable porphyrin@SPION nanospheres exhibited multifunction of both photodynamic potential and smart magnetic targeting. Among these newly prepared nanospheres, dicationic porphyrin@SPION nanospheres have smart pH-responsive release, high cell uptake activity, targeted cell accumulation as well relatively high photodynamic cytotoxicity to HeLa cells. The drug delivery for porphyrin@SPION was

evidenced to be relatively safe by monitoring the interactions between the nanospheres and HSA in the blood plasma. Despite of numerous reports on the SPION-loading of neutral porphyrins, as far as we know, this is the first time to shed lights on the loading of cationic porphyrins to SPION nanospheres and evaluate their cytotoxicity as bio-safety in delivery. We suppose this contribution will facilitate the discovery of new targeted anticancer drugs and promote the research of bio-safety evaluation of the loaded agents.

## Acknowledgements

The author(s) disclosed receipt of the following financial support for the research, authorship, and/or publication of this article: this work was financially supported by the Natural Science Foundation of Guangdong (2016A030313807) and the Outstanding Young Teachers' Foundation in Colleges and Universities of Guangdong Province.

## Notes and references

- 1 S. L. Gai, C. X. Li, P. P. Yang and J. Lin, *Chem. Rev.*, 2014, **114**, 2343.
- 2 X. Liang, X. Li, L. Jing, X. Yue and Z. Dai, *Biomaterials*, 2014, **35**, 6379.
- 3 U. S. Chung, J. H. Kim, B. Kim, E. Kim, W. D. Jang and W. G. Koh, *Chem. Commun.*, 2016, **52**, 1258.
- 4 S. Endo, N. Kudo, S. Yamaguchi, K. Sumiyoshi, H. Motegi, H. Kobayashi, S. Terasaka and K. Houkin, *Ultrasound. Med. Biol.*, 2015, **41**, 2458.
- 5 R. Hiramatsu, S. Kawabata, S. Miyatake, T. Kuroiwa, M. W. Easson and M. G. Vicente, *Lasers Surg. Med.*, 2011, **3**, 52.
- 6 S. Singh, A. Aggarwal, N. V. S. D. K. Bhupathiraju, G. Arianna, K. Tiwari and C. M. Drain, *Chem. Rev.*, 2015, **115**, 10261.
- 7 D. R. McMillin, A. H. Shelton, S. A. Bejune, P. E. Fanwick and R. K. Wall, *Coord. Chem. Rev.*, 2005, **249**, 1451.
- 8 P. Zhao, M. C. Liu, M. Zheng, S. F. Jin, D. T. Tang, J. Chen, Y. N. Ma, J. Q. Lin, X. H. Wang and H. J. Liu, *Dyes Pigm.*, 2016, **128**, 41.
- 9 P. Zhao, S. F. Jin, J. Z. Lu, M. Zheng, J. L. Lv, J. Q. Wu, P. P. Chen, C. L. Tan and D. W. Chen, *Spectrochim. Acta, Part A*, 2015, **137**, 227.
- 10 S. F. Jin, P. Zhao, L. C. Xu, M. Zheng, J. Z. Lu, P. L. Zhao, Q. L. Su, H. X. Chen, D. T. Tang, J. Chen and J. Q. Lin, *Bioorg. Chem.*, 2015, **60**, 110.
- 11 H. Yao, H. Sasahara and K. Kimura, *Chem. Mater.*, 2011, **23**, 913.
- 12 W. Li, W. Lu, Z. Fan, X. Zhu, A. Reed, B. Newton, Y. Zhang, S. Courtney, T. P. Tiyyagura, S. Li, E. Butler, H. Yu, C. P. Ray and R. Gao, *J. Mater. Chem.*, 2012, **22**, 12701.
- 13 Y. M. Zhou, X. L. Liang and Z. F. Dai, *Nanoscale*, 2016, **8**, 12394.
- 14 W. Li, N. Gandra, E. Ellis, S. Courtney, S. Li, E. Butler and R. Gao, *ACS Appl. Mater. Interfaces*, 2009, **1**, 1778.
- 15 Z. Li, J. Wang, J. Chen, J. Lei, X. Wang and B. Zhang, *Nanotechnology*, 2010, **21**, 102.
- 16 U. Karel, H. Katerina, S. Vladimir, B. Aristides, T. Jiri and Z. Radek, *Chem. Rev.*, 2016, **116**, 5338.
- 17 Y. R. Pelgrift and J. A. Friedman, *Adv. Drug Delivery Rev.*, 2013, **65**, 1803.
- 18 S. Marvin, *Calculator Plugins were used for pKa calculation, ChemAxon 5.0.1*, 2008.
- 19 A. D. Adler, F. R. Longo, J. D. Finarelli, J. Assour and L. Korsakoff, *J. Org. Chem.*, 1967, **32**, 476.
- 20 I. Kraljić and S. E. I. Mohsni, *Photochem. Photobiol.*, 2008, **28**, 577.
- 21 S. Santra, R. Tapeç, N. Theodoropoulou, J. Dobson, A. A. Hebard and W. H. Tan, *Langmuir*, 2001, **17**, 2900.
- 22 I. F. Tannock and D. Rotin, *Cancer Res.*, 1989, **49**, 4373–4384.
- 23 M. Massignani, C. LoPresti, A. Blanzas, J. Madsen, S. P. Armes, A. L. Lewis and G. Battaglia, *Small*, 2009, **5**, 2424.
- 24 G. Ding, G. Yi, Y. Lv, X. Liu, X. Li and X. Zhang, *Colloids Surf., B*, 2012, **91**, 68.
- 25 S. Walia, S. Sharma, P. M. Kulurkar, V. Patial and A. Acharya, *Int. J. Pharm.*, 2016, **498**, 110.
- 26 K. Kano, H. Minamizono, T. Kitae and S. Negi, *J. Phys. Chem. A*, 1997, **101**, 18.
- 27 P. Zhao, J. W. Huang, W. J. Mei, J. He and L. N. Ji, *Spectrochim. Acta, Part A*, 2010, **75**, 1108.
- 28 L. Nastassja, C. Vicki and D. Rebekah, *Small*, 2008, **4**, 26.
- 29 P. Zhao, J. Z. Lu, J. He, H. C. Wang, P. P. Chen, D. W. Chen and Q. Y. Bin, *Nucleosides, Nucleotides Nucleic Acids*, 2014, **33**, 597.
- 30 Y. Ye, X. L. Chen and Y. Guo, *Adv. Mater. Res.*, 2013, **749**, 471.
- 31 X. Zhao, R. Liu, Z. Chi, Y. Teng and P. Qin, *J. Phys. Chem. B*, 2010, **114**, 5625.
- 32 H. C. Wang, X. H. Jiang, L. M. Zhou, Z. J. Chen, W. M. Yin, M. Duan, P. L. Liu and X. M. Jiang, *J. Lumin.*, 2013, **134**, 138.
- 33 Y. H. Liu, F. Y. Ji and R. T. Liu, *Nanotoxicology*, 2013, **7**, 97.
- 34 P. Zhao, J. W. Huang and L. N. Ji, *Spectrochim. Acta, Part A*, 2012, **88**, 130.
- 35 M. C. Liu, S. F. Jin, M. Zheng, Y. Wang, P. L. Zhao, D. T. Tang, J. Chen, J. Q. Lin, X. H. Wang and P. Zhao, *J. Biomater. Appl.*, 2016, **31**, 261.
- 36 M. R. Eftink and C. A. Ghiron, *Anal. Biochem.*, 1981, **114**, 199.
- 37 J. R. Lakowicz and G. Weber, *Biochemistry*, 1973, **12**, 4161.
- 38 X. L. Lu, J. J. Fan, Y. Liu and A. X. Hou, *J. Mol. Struct.*, 2009, **934**, 1.
- 39 Z. D. Qi, B. Zhou, X. Qi, C. Shi, Y. Liu and J. Dai, *J. Photochem. Photobiol., A*, 2008, **193**, 81.
- 40 T. Nekira, K. Tshihara, K. Matsuo, S. Izumi, T. Yamazaki and A. Ishida, *Anal. Biochem.*, 2012, **430**, 179.
- 41 T. Peters and A. Serum, *Advances in Protein Chemistry*, Longman, New York, 1985.
- 42 X. M. He and D. C. Carter, *Nature*, 1992, **358**, 209.
- 43 T. Chakraborty, I. Chakraborty, S. P. Moulik and S. Ghosh, *Langmuir*, 2009, **25**, 3062.
- 44 X. Qu, C. Yang, J. Zhang, N. Ding, Y. Lu, L. Huang and G. Xiang, *J. Drug Targeting*, 2010, **18**, 351.